

Understanding the β -K₂CO₃-Type Na(Na_{0.5}Sc_{0.5})BO₃:Ce₃ + Phosphor

To cite this article: Jiyou Zhong et al 2021 ECS J. Solid State Sci. Technol. 10 096014

View the <u>article online</u> for updates and enhancements.

Visualize the processes inside your battery! Discover the new ECC-Opto-10 and PAT-Cell-Opto-10 test cells!



- Battery test cells for optical characterization
- High cycling stability, advanced cell design for easy handling
- For light microscopy and Raman spectroscopy

www.el-cell.com +49 (0) 40 79012 734 sales@el-cell.com







Understanding the β -K₂CO₃-Type Na(Na_{0.5}Sc_{0.5})BO₃:Ce₃ + Phosphor

Jiyou Zhong,¹ Ya Zhuo,² Hongshi Zhang,¹ Weiren Zhao,^{1,z} Jun Wen,^{3,z} and Jakoah Brgoch^{2,*,z}

A Na(Na_{0.5}Sc_{0.5})BO₃:Ce³⁺ phosphor in the β -K₂CO₃-type crystal structure was developed by identifying orthoborate substitutional derivatives with distinct crystal and electronic structure and high structural rigidity. Crystal structure and compositional analysis after the high-temperature synthesis of the target phase confirmed the product's phase purity. Photoluminescence spectroscopy revealed a bright blue emission centered at 420 nm under 340 nm excitation. Computational modeling indicated that the optical properties stem from Ce³⁺ having a significant site preference for the eight-coordinated Na⁺ crystallographic site rather than the smaller six-coordinated Na⁺/Sc³⁺ site. Analyzing the local crystal structure through a combined computational and spectroscopic analysis showed that the substitution of Ce³⁺ on the normally eight-coordinated site causes an unexpected evolution of the crystal structure resulting in a nine-coordinated rare-earth position leading to the blue emission. These results highlight the importance of using a combined computational and experimental evaluation to develop new phosphors and understand their ensuing complex optical properties.

© 2021 The Electrochemical Society ("ECS"). Published on behalf of ECS by IOP Publishing Limited. [DOI: 10.1149/2162-8777/ac2780]

Manuscript submitted July 23, 2021; revised manuscript received September 2, 2021. Published September 27, 2021. This paper is part of the JSS Focus Issue on Focus Issue Dedicated to the Memory of George Blasse: Recent Developments in Theory, Materials, and Applications of Luminescence.

Phosphor-converted white-light-emitting diodes (pc-WLEDs) have received significant attention due to their superior performance, such as high luminous efficacy, long operating lifetimes, and environmentally benign components compared to traditional incandescent or compact fluorescent light bulbs. 1-3 Most low-priced commercial pc-WLEDs available today are fabricated using Y₃Al₅O₁₂:Ce³⁺ yellow phosphor coated on top of a blue-emitting InGaN LED chip. This combination of luminescent materials creates a functional white light, even though the device suffers from a poor color-rendering index (Ra < 75) and a high correlated color temperature (CCT > 4500 K) due to the lack of a considerable red spectral component.^{4–7} UV or violet LED chips emitting in the 340-420 nm range coated with blue, green, and red phosphors have been suggested as an alternative method to produce high-quality white light with similar luminous efficacy, even higher color-rendering, and superior color uniformity. 8–10 However, few phosphors meet the demands necessary to realize this new device architecture. Indeed, one of the essential needs for UV-based fullspectrum LED lighting is the discovery of an efficient broadband blue-emitting phosphor that can cover the 400 nm to 500 nm region. Unfortunately, the best commercially available blue-emitting $BaMgAl_{10}O_{17}$: Eu^{2+} (full width at half-maximum = 55 nm) is not broad enough to cover the entire blue to cyan region, spurring the search for new UV-based phosphors. 11-13

Multiple phosphors have been recently developed by analyzing the crystal chemistry of natural mineral prototypes. ¹⁴ One particular system that has become synonymous with phosphor discovery is the prolific β –type crystal structures. Phosphors that fall in this category include the β –K₂SO₄ structure-type of the (Ba_{2-x}Sr_x)SiO₄:Eu²⁺ system, ¹⁵ the β –Al₂O₃ type BaMgAl₁₀O₁₇:Eu²⁺ compound, ¹⁶ and the green-emitting β –SiAlON:Eu²⁺. ¹⁷ These compounds have garnered considerable interest in the phosphor field, and many have even found commercial applications. The advantage of these β –phase structure-type compounds stems from the highly symmetric crystal systems and ordered crystallographic arrangements that generate high emission efficiency upon rare-earth substitution.

based on the β -K₂CO₃- type mineral structure. ¹⁸ This includes the β -K₂CO₃-type derived NaMBO₃ (M = Mg, Ca, Sr, Ba) orthoborate family, which crystallizes in different space groups depending on the M cation but possesses a similar atomic arrangement and coordination environment, making them part of a broader system. All of these compounds exhibit unique optical properties when substituted with Ce³⁺. For instance, the analogs NaCaBO₃:Ce³⁺, NaSrBO₃:Ce³⁺, and NaBaBO₃:Ce³⁺ adopt space group *Pmmn*, *P*2₁/c, and *C*2/m, respectively, and are efficient blue-emitting (~425 nm) phosphors with photoluminescent quantum yields (PLQY) of $68 \sim 75\%$ under ultraviolet (\sim 360 nm) excitation. The origin of the optical properties is due to Ce³⁺ substituting on the nine-coordinated alkaline-earth ion site. 19-22 Disappointingly, these phosphors suffer from poor thermal stability, with the emission intensity of these three phases decreasing by more than 50%, going from 300 K to 423 K, which limits their practical applications. NaMgBO₃:Ce³⁺ crystallizes in space group C2/c and is a blue-cyan-emitting (\sim 480 nm) material with a much higher PLQY (>90%) and nearly zero-thermal quenching at 423 K. These optical properties stem from Ce³⁺ occupying the slightly different 8-coordinated Na+ site instead of the larger 9-coordinated site. 23 As a result, NaMgBO₃:Ce³⁺ is a promising candidate for applications in full-spectrum LED lighting. Therefore, it is reasonable to search for additional potentially notable phosphors by identifying compounds that adopt the β -K₂CO₃-type system and have a similar crystal structure to NaMgBO₃:Ce³-

Another class of β -type phosphors also recently discovered was

There remains one reported orthoborate compound that crystallizes with the β – K_2CO_3 -type structure that has not been investigated as a phosphor. Na(Na_{0.5}Sc_{0.5})BO₃, which was first identified by Fang et al., and has a close relationship with β -type NaMgBO₃. Before synthesizing this phase, the crystal structure, electronic structure, and structural rigidity were examined to evaluate the possibility of this system as a rare-earth substituted phosphor host. Based on the promising computational analysis, the target compound was prepared using high-temperature ceramic synthesis and characterized using powder X-ray diffraction and electron microscopy. The subsequent optical property analysis of the Ce³⁺-substituted compound showed an anomalous emission peak, which was understood through a combination of experiment and DFT calculations. These results highlight the importance of revealing the relationship

¹School of Physics and Optoelectronic Engineering, Guangdong University of Technology, Guangzhou 510006, People's Republic of China

²Department of Chemistry, University of Houston, Houston, Texas 77204, United States of America

³School of Physics and Electronic Engineering, Anqing Normal University, Anqing 246133, People's Republic of China

^{*}Electrochemical Society Member.

^zE-mail: zwren123@126.com; wenjunkd@mail.ustc.edu.cn; jbrgoch@uh.edu

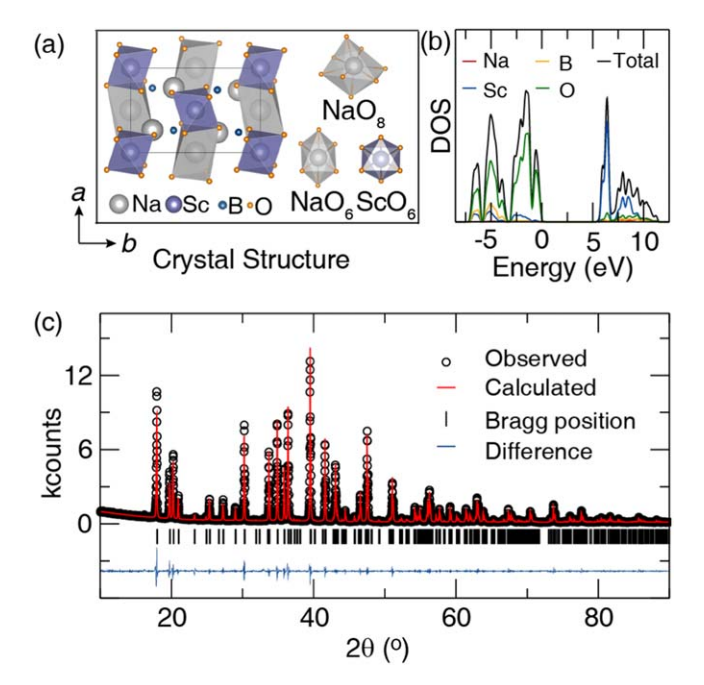


Figure 1. (a) Crystal structure of $Na(Na_{0.5}Sc_{0.5})BO_3$ host with the coordination environments of the Na^+ and Sc^{3+} ions highlighted. (b) The projected total density of states (DOS) of $Na(Na_{0.5}Sc_{0.5})BO_3$ calculated with the hybrid functional, HSE06. (c) The powder X-ray diffractograms and Le bail refinement of the as-prepared $Na(Na_{0.5}Sc_{0.5})BO_3$ sample.

between crystal structures and optical properties through a combination of experiment and computational analysis.

Experiment and Methodology

Computation.—The crystal structure of Na(Na_{0.5}Sc_{0.5})BO₃ was optimized using the Vienna ab initio Simulation Package (VASP),² which is a plane-wave pseudopotential total energy package based on density functional theory (DFT).^{25–28} The atomic positions and lattice parameters were relaxed with electronic convergence criteria of 1×10^{-5} eV and atomic convergence criteria 0.01 eV Å cutoff energy of 500 eV was used for the basis set of the plane waves, and an 8 \times 4 \times 4 Γ -centered Monkhorst-Pack k-point grid was used to sample the first Brillouin zone. The Debye temperature (Θ_D) was determined using the elastic constants obtained from density functional perturbation theory and the arithmetic relations quasi-harmonic outlined by the Debye model. Perdew-Burke-Ernzerhof (PBE) exchange-correlation functional was employed for structure optimization and the elastic constant calculations, while the subsequent electronic properties were determined using the HSE06 hybrid functional.²⁹ The possibility of neutral defects was examined by calculating the formation energy using the PBE0 hybrid functional.

The energies and relative oscillator strengths of the $4\,\mathrm{f} \to 5\mathrm{d}$ transitions of $\mathrm{Ce^{3+}}$ ions were then calculated using crystal structures optimized with PBE0, constructed with $\mathrm{Ce^{3+}}$ -centered defect clusters, i.e., $[\mathrm{CeO_6}]^{9-}$ and $[\mathrm{CeO_9}]^{15-}$, embedded in the Na(Na_{0.5}Sc_{0.5})BO₃ host crystal structure. Wave function-based embedded cluster ab initio calculations as implemented in the MOLCAS program were then performed. Accurate quantum chemical ab initio calculations were used to treat the valence electrons of the atoms in the defect clusters, whose immediate lattice environments were represented by the embedding ab initio model potentials (AIMPs) located at the host lattice sites within a 10.0 Å spherical radius. Point charges were situated at lattice sites within a sphere of the radius 50.0 Å used to represent the lattice environments outside of the AIMPs. The CASSCF/CASPT2/RASSI-SO methods utilized in the embedded cluster calculations also

include the effects of the spin-orbit coupling and second-order perturbation correction, ³² and, thus, give reasonably accurate energies and wavefunctions of the 4 f and 5d states for the Ce³⁺ ion.

Synthesis.—The Na(Na_{0.5}Sc_{0.5})BO₃:xCe³⁺ (x = 0, 0.01, 0.02, 0.03, 0.04, and 0.05) series was prepared with varying rare-earth concentration using a high-temperature, solid-state chemical route. The starting materials included NaHCO₃ (Aldrich, 99.95%), Sc₂O₃ (Aldrich, 99.9%), H₃BO₃ (Aldrich, 99.9%), and CeO₂ (Aldrich, 99.99%). The powders were weighed according to the required stoichiometric ratios plus 3% excess H₃BO₃ and 3% excess NaHCO₃ to compensate for evaporation during synthesis. The powders were mixed using an agate mortar and pestle, and the homogeneous starting materials were placed in an alumina crucible, fired at 923 K using a 3 K min⁻¹ heating rate, and held for 8 h to decompose H₃BO₃ and NaHCO₃. The powders were then cooled to room temperature (3 K min⁻¹), reground, and re-heated to 1163 K for 6 h (3 K min⁻¹ heating and cooling) under a flowing reducing atmosphere (15% H₂/85% N₂). The final products were ground into a fine powder using an agate mortar and pestle.

Characterization.—X-ray diffractograms (X'Pert3 PANalytical; Cu K α , $\lambda=1.5406$ Å) were collected to confirm the phase purity of each product. Scanning electron microscopy (SEM) was used to image the particles, and energy dispersive X-ray spectroscopy (EDS) was employed to map the location of the elements. The micrographs were collected on a Hitachi-S4800 (Japan). The room temperature photoluminescence, temperature-dependent photoluminescence spectra, and the time-gated photoluminescence decay curves of the Ce³⁺ substituted phosphors were then collected using an FLS-980 fluorescence spectrophotometer (Edinburgh Instruments) equipped with a Xenon flash lamp (450 W, Osram) as the excitation source. The quantum yields were measured using the integrating sphere on the Fluorolog-3 (HORIBA, USA), and a Xe lamp was used as an excitation source with BaSO₄ powder as a reference.

Results and Discussion

Selecting $Na(Na_{0.5}Sc_{0.5})BO_3$ as a possible phosphor host.— Na(Na_{0.5}Sc_{0.5})BO₃ was first reported as Na₃ScB₂O₆ and proposed to adopt the monoclinic crystal system with space group $P2_1/c$ (no. 14). 33 The crystal structure of this phase features a three-dimensional framework composed of trigonal planer [BO₃] units, hexagonal bipyramid [NaO₈] units, and two distorted octahedral [ScO₆] and [NaO₆] units, as illustrated in Fig. 1a. This structure-type is closely related to NaMgBO₃ in the β -K₂CO₃ structure-type, which crystallizes in a similar monoclinic crystal system but a different space group (C2/c, no. 15). The main difference between the structures is that the divalent magnesium octahedral units are split into an ordered monovalent octahedron and a trivalent octahedron. The NaMgBO₃ system was shown to generate a highly efficient blue-cyan-emitting phosphor when Ce^{3+} substituted on the eight-coordinated Na^+ site. The same work showed Ce^{3+} does not occupy the smaller six-coordinated Mg^{2+} site due to a combination of the charge mismatch and size discrepancy between Ce³⁺ and Mg^{2+,23} In the analogous Na(Na_{0.5}Sc_{0.5})BO₃ system, Ce³⁺ is also expected to enter the eight-coordinated Na⁺ site in Na(Na_{0.5}Sc_{0.5})BO₃ because the octahedral Na⁺/Sc³⁺ sites likely remain too small for Ce³⁺ to occupy. Therefore, a similar blue or cyan emission was expected for $Na(Na_{0.5}Sc_{0.5})BO_3:Ce^{3+}$

Given the interest in this system as a possible phosphor host, the electronic structure and structural rigidity of Na(Na_{0.5}Sc_{0.5})BO₃ were first examined via DFT calculation. The structural rigidity, estimated based on the materials $\Theta_{\rm D}$, is widely believed to be related to the PLQY.^{34–36} Generally, phosphors with a higher $\Theta_{\rm D}$ tend to exhibit higher-energy phonon modes that decrease the probability of non-radiative relaxation and thus induce an increased photoluminescence quantum yield. The $\Theta_{\rm D}$ of the Na(Na_{0.5}Sc_{0.5})BO₃ host was calculated to be 545 K using the DFT-PBE method within the quasi-

Table I. The refined crystal structure data obtained by using the Le Bail method.

Formula	$Na(Na_{0.5}Sc_{0.5})BO_{2}$
Radiation type; λ (Å)	X-ray; 1.5406
2θ range (°)	10–90
Temperature (°C)	25
Space group	$P2_{1}/c$
a (Å)	5.0944(9)
b (Å)	8.9798(4)
c (Å)	7.1128(3)
$\beta(\circ)$	123.96(8)
Unit cell volume (Å ³)	269.89(7)
Profile R -factor, R_p	0.0595
Weighted profile R -factor, R_{wp}	0.0883
χ^2	4.091

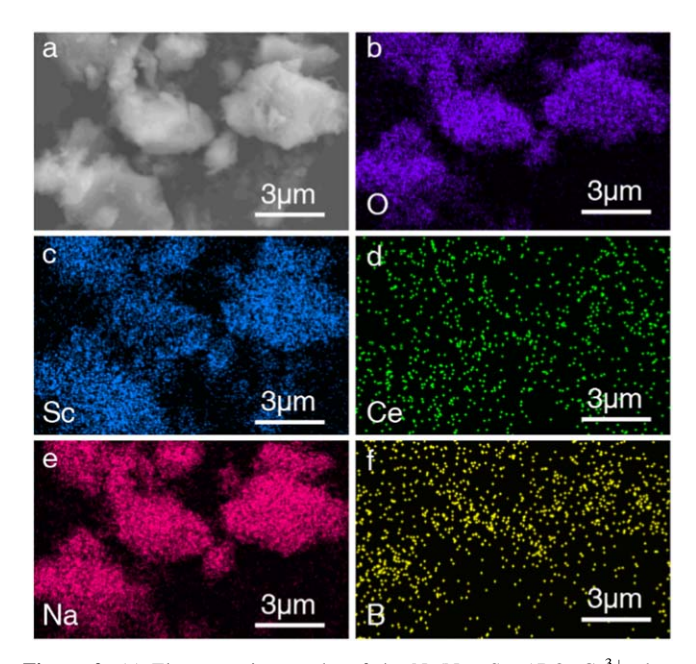


Figure 2. (a) Electron micrographs of the Na(Na_{0.5}Sc_{0.5})BO₃:Ce³⁺ phosphor particles, and (b)–(f) EDS elemental mappings of the selected particles for Na, Sc, B, O, and Ce, respectively.

harmonic Debye model.³⁷ This value is slightly lower than NaMgBO $_3$ (563 K) but much higher than blue-emitting phosphor hosts such as Ba $_2$ SiO $_4$ (305 K) and BaMgAl $_{10}$ O $_{17}$ (478 K).^{34,37} This suggests that rare-earth substitution in Na(Na $_{0.5}$ Sc $_{0.5}$)BO $_3$ may potentially achieve a high PLQY.

The band gap of the host crystal structure must also be sufficiently wide to mitigate photo- or thermal- ionization, which is critical for thermal stability. The density of states (DOS) for Na(Na_{0.5}Sc_{0.5})BO₃ was calculated using the HSE06 hybrid functional (Fig. 1b), resulting in a computed band gap ($E_{\rm g,HSE}$) of $\approx 5.2~{\rm eV}$. This is slightly smaller than NaMgBO₃ (5.5 eV), ²³ but still sufficiently wide to limit the most common quenching pathways. Decomposing the electronic structure into the partial density of states shows that the O 2p states consist of the top of the valence band, while unoccupied Sc 3d states set the bottom of the conduction band. A relatively strong hybridization between the O 2p and Sc 3d in the conduction band was also observed. The DFT investigation suggested that Na(Na_{0.5}Sc_{0.5})BO₃ is a rigid crystal structure based on θ_D with a sufficiently wide band gap to make this phase a phosphor host candidate.

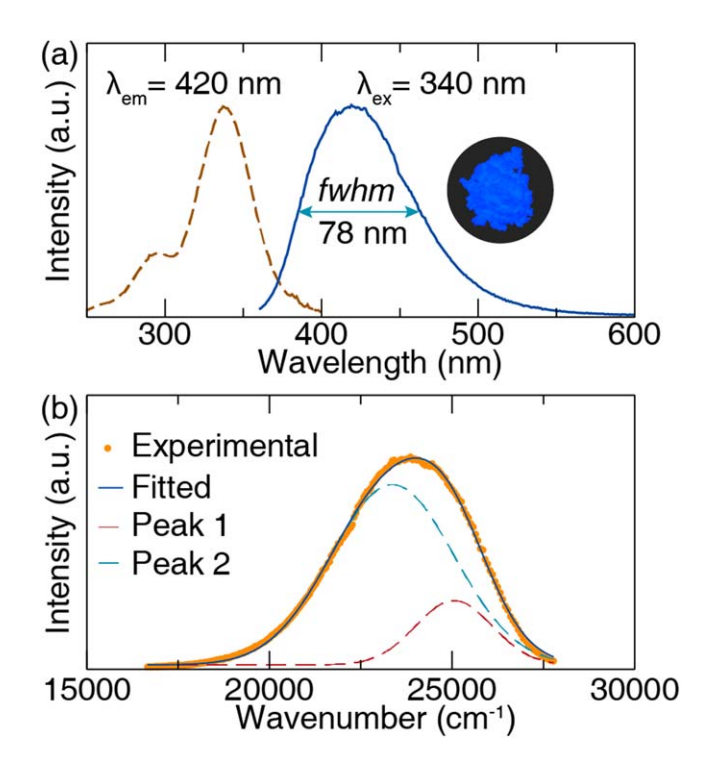


Figure 3. (a) Photoluminescent excitation and emission spectra of $Na(Na_{0.5}Sc_{0.5})BO_3$: Ce^{3+} containing 3 mol% rare-earth at room temperature. The inset presents a photograph of this phosphor under a 365 nm lamp. (b) Two Gaussian bands describe the spin–orbit coupled relaxation observed in the emission spectrum.

Synthesis and photoluminescence properties $Na(Na_{0.5}Sc_{0.5})BO_3:Ce_3$ —The Ce³⁺-substituted Na(Na_{0.5}Sc_{0.5})BO₃ phosphor was chosen for synthesis based on the calculated properties. The product was prepared using a two-step high-temperature synthetic route. The powder X-ray diffractogram and whole-pattern Le Bail refinement of the Na(Na_{0.5}Sc_{0.5})BO₃ host is shown in Fig. 1c. The results of the Le Bail refinement, provided in Table I, support the phase purity and confirm the crystal structure. The Ce³⁺-substituted product's morphology was also examined by SEM. Fig. 2a. shows that the particles are generally irregular in shape with an average size of several microns. Mapping the elemental distribution using energy-dispersive X-ray spectrometry (EDS) (shown as Figs. 2b-2f) shows that only the loaded starting elements are present in the product. The Na, Sc, B, O, and Ce are also uniformly distributed within the particles examined.

The photoluminescent excitation and emission spectra of Na(Na_{0.5}Sc_{0.5})BO₃: Ce³⁺ phosphor are plotted in Fig. 3a. The excitation spectrum (monitored at $\lambda_{\rm em} = 420 \, \rm nm$) spans from 250 to 400 nm with two peaks centered at 295 and 340 nm ascribed to electronic transitions from the 4 f ground state to different excited states of the Ce^{3+} 5d orbitals. Under ultraviolet light excitation (λ_{ex} = 340 nm), this phosphor exhibits an intense broad emission band (as shown in the inset of Fig. 3a) centered at 420 nm with a full width at half maximum (fwhm) of 78 nm (4376 cm⁻¹), similar to $NaBaBO_3:Ce^{3+}$ (420 nm) and $NaSrBO_3:Ce^{3+}$ (424 nm). The blue emission of $Na(Na_{0.5}Sc_{0.5})BO_3:Ce^{3+}$ suggests the rare-earth ion is experiencing a weak crystal field splitting environment making the larger polyhedral volume site of [NaO₈], which is the most likely substitution position. The emission spectra can be deconvoluted into two Gaussian sub-bands (depicted in Fig. 3b) with peaks centered at 398 nm (25125 cm⁻¹) and 429 nm (23310 cm⁻¹), respectively. The energy difference (Δk) between these two Gaussian peaks is 1815 cm⁻¹, which agrees with the expected difference between the ground state ${}^{2}F_{7/2}$ and ${}^{2}F_{5/2}$ levels (1800–2000 cm⁻¹) of Ce³⁺.40

Additional information about this phosphor can be gained by analyzing the emission spectrum of Na(Na_{0.5}Sc_{0.5})BO₃:Ce³⁺ with

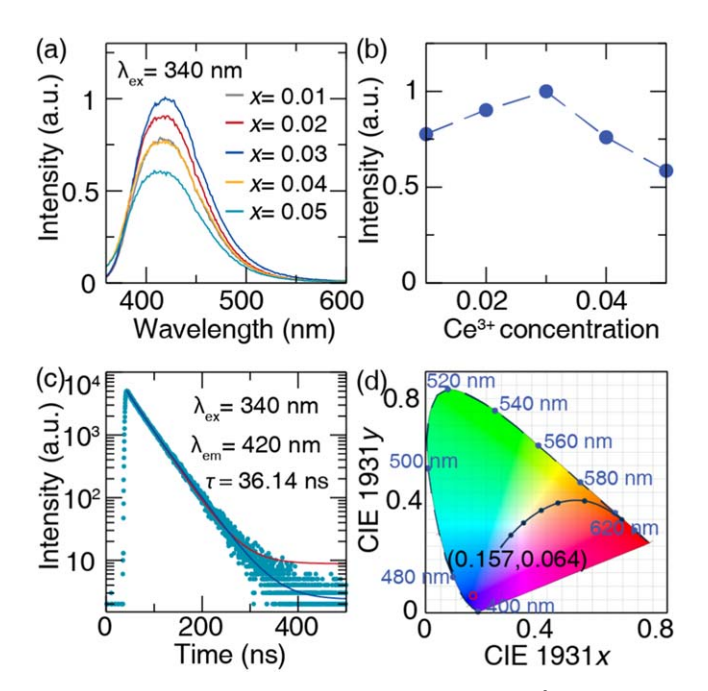


Figure 4. (a) Emission spectra of Na(Na_{0.5}Sc_{0.5})BO₃:xCe³⁺ (x = 0.01 - 0.05) phosphors under 340 nm excitation at room temperature; (b) relative emission intensity of Na(Na_{0.5}Sc_{0.5})BO₃:Ce³⁺ phosphor as function of Ce³⁺ concentration; (c) room temperature photoluminescence lifetime decay curve of Na(Na_{0.5}Sc_{0.5})BO₃:Ce³⁺ (3 mol% rare-earth) excited at 340 nm with the mono-exponential (red) and bi-exponential (blue) function fits shown; (d) CIE coordinates of Na(Na_{0.5}Sc_{0.5})BO₃:Ce³⁺ (3 mol% rare-earth) excited by 340 nm.

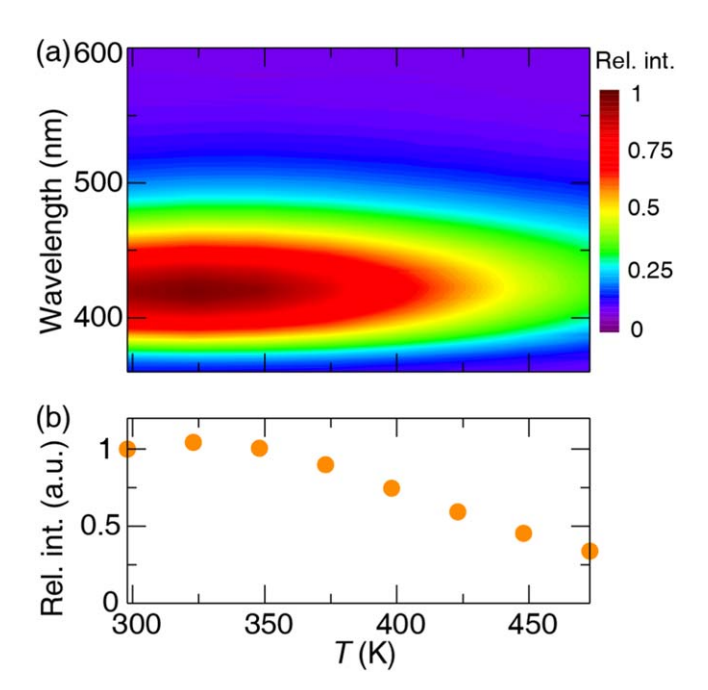


Figure 5. (a) Contour plot of the emission spectra of $Na(Na_{0.5}Sc_{0.5})BO_3$: Ce^{3+} (3 mol% rare-earth) phosphor excited at 340 nm as a function of temperature. (b) The relative peak intensity of the emission spectra as a function of temperature.

varying Ce³⁺ concentrations (1 mol% to 5 mol%). Collecting these data under 340 nm excitation, as plotted in Fig. 4a, shows the phosphor slightly blue shifts with increasing Ce³⁺ concentration. This change is commonly explained by the gradual weakening of the crystal field around Ce³⁺ caused by lattice expansion with increasing Ce³⁺ content. The emission intensity as a function of Ce³⁺

concentration (shown as Fig. 4b) first increases to a maximum and then decreases; the optimized doping concentration is about x=0.03 (with PLQY value of 48.6% under 340 nm excitation), beyond which concentration quenching occurs.

Time-resolved photoluminescence decay curves for Na(Na_{0.5}Sc_{0.5})BO₃:Ce³⁺were also collected under 340 nm excitation at room temperature to probe the optical properties. Figure 4c presents the decay curve for the 3 mol% Ce³⁺ substitution monitored at 420 nm under 340 nm excitation. The decay curve slightly deviates from a monoexponential function but fits well with a biexponential function producing lifetimes of $\tau_1 = 17.2 \, \mathrm{ns}$ and $\tau_2 =$ 41.3 ns, or an average lifetime $\tau_{\rm ave.} = 36.14$ ns. A similar situation was also observed in NaMgBO₃:Ce³⁺ and suggested to stem from changes in the local structure of the Ce³⁺ sites.²³ It is also possible that the dual lifetime arises from the presence of defects in the crystal structure, with the faster lifetime (au_1) appearing from defectassociated luminescence and τ_2 coming from the rare-earth ion. Nevertheless, similar τ_2 lifetimes were also observed in the analogous NaBaBO₃:Ce³⁺ (36.2 ns).^{20,22} Finally, and NaSrBO₃:Ce³⁺ (35.33 ns)the CIE coordinates Na(Na_{0.5}Sc_{0.5})BO₃:0.03Ce³⁺ under 340 nm excitation, as illustrated in Fig. 4d, were calculated to be (0.157, 0.064), revealing a deep blue color of this phosphor upon ultraviolet excitation.

The thermal quenching properties of this phosphor were also evaluated. The temperature-dependent emission spectra of the Na(Na_{0.5}Sc_{0.5})BO₃: Ce³⁺ phosphor containing 3 mol% of the rare-earth ion were collected from 298 to 473 K under 340 nm excitation. The contour plot of emission spectra and normalized peak intensity as a function of temperature are plotted in Fig. 5. The relative emission intensity was found to stay constant (or a very slight increase) with increasing temperature up to 323 K. Further increasing the temperature causes thermal quenching to take over, resulting in the loss of emission intensity. The T_{50} , which is the temperature that the emission intensity of a phosphor has decreased to 50% of the initial value, was found to be 436 K. This is also close to the analogous systems, NaBaBO₃:Ce³⁺ (415 K) and NaSrBO₃:Ce³⁺ (423 K). $^{20-22}$

Site occupation, local structure evolution, and spectroscopic analysis.—Although Na(Na_{0.5}Sc_{0.5})BO₃ has a similar crystal structure to NaMgBO₃, the title phosphor presents different optical properties than predicted. In fact, the photoluminescence excitation and emission, lifetime decay, and thermal quenching properties more closely match the NaMBO₃: Ce^{3+} (M = Sr, Ba) phosphor series rather than NaMgBO3:Ce3+. This discrepancy was examined by determining the site preference of Ce³⁺ by calculating the formation (substitution) energy of Ce³⁺ entering the different sites (Fig. 6a). There are three possible substitution patterns considered for this crystal structure include Ce_{Sc} (Ce^{3+} entering into Sc^{3+} site), $Ce_{Na(dod)} \bullet \bullet + Na_{Sc}$ " (Ce^{3+} entering into eight-coordinated dodecahedral Na⁺ site and an additional Na⁺ entering into Sc³⁺ site), and Ce_{Na(oct)}••+ Na_{Sc}" (Ce³⁺ entering into six-coordinated octahedral Na⁺ site and an additional Na⁺ entering into Sc³⁺ site). From the calculations, Ce³⁺ occupying the six-coordinated Na⁺ site can automatically be excluded because it has noticeably higher formation energy, whereas Ce³⁺ entering the eight-coordinated Na⁺ site has the lowest energy. The model where Ce^{3+} enters the Sc^{3+} site has slightly higher formation energy, which suggests it may be possible to stabilize the substitution of Ce³⁺ for Sc³⁺ under a specific synthesis condition.

 Ce^{3+} occupying the eight-coordinated Na^+ site, however, would be expected to generate optical properties similar to $NaMgBO_3:Ce^{3+}$, which was not observed here. A closer examination of the computationally optimized coordination environment around Ce^{3+} indicates the crystal structure evolves from the 8-coordinated position into a $[CeO_9]$, shown in Fig. 6b. This is structurally similar to Ce^{3+} occupying the 9-coordinated M^{2+} site in the $NaMBO_3:Ce^{3+}$ (M=Sr, Ba) series. Thus, it is easy to understand the comparable luminescence of these systems because

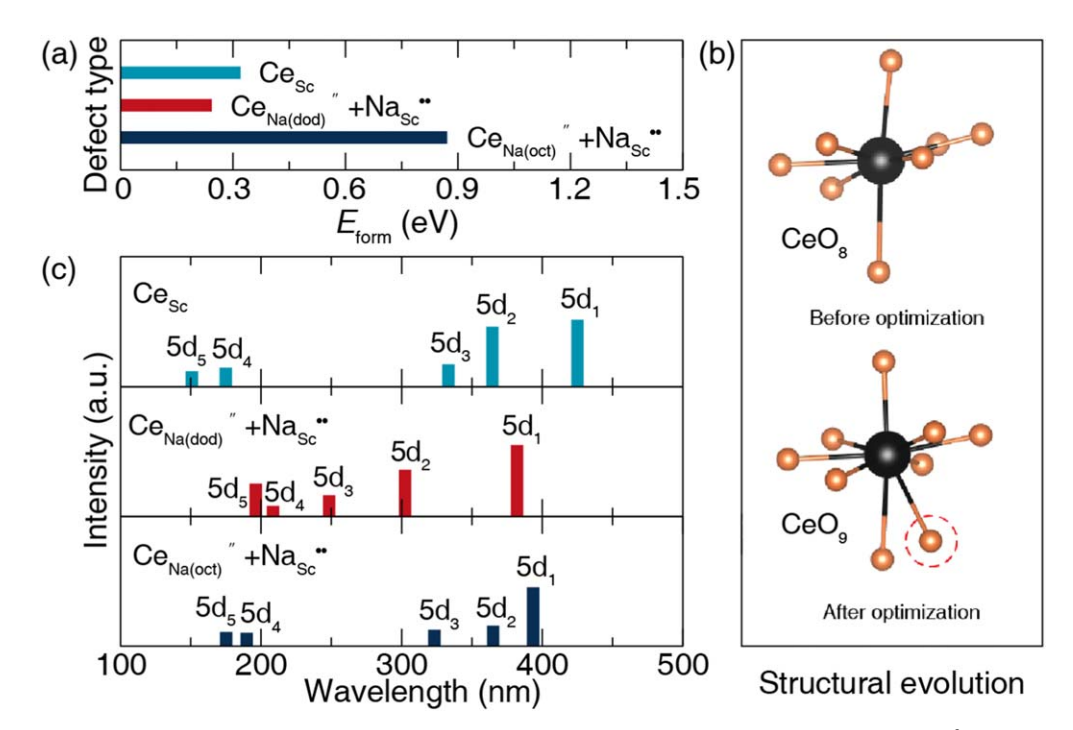


Figure 6. (a) calculated relative defect formation energies using the hybrid functional. (b) Coordination environment around Ce^{3+} evolving into [CeO_9] through optimizing Ce^{3+} in eight-coordinated Na^+ site. The oxygen highlighted in red emerges after optimization. (c) calculated relative oscillator strengths of $4 \text{ f} \rightarrow 5 \text{d}$ transitions of Ce^{3+} in different crystallographic sites in $Na(Na_{0.5}Sc_{0.5})BO_3$.

of the similar structure type and local coordination environment around Ce^{3+} . Moreover, comparing the lattice parameters of the DFT hybrid functional optimized crystal structure containing the $Ce_{Na(dod)}$ ··+ Na_{Sc} " defect with the unsubstituted $Na(Na_{0.5}Sc_{0.5})BO_3$ unit cell shows a notable expansion (Table II), which provides evidence for the observed blue-shift with increasing Ce^{3+} concentration induced by a lattice expansion. Lastly, the bi-exponential decay curve is reasonable because the calculated changes in the local crystal structure around Ce^{3+} suggest both complete 9-coordinated Ce^{3+} accompanied by anti-site defects that change the coordination environment.

The rare-earth substitution site was further supported by simulating the 4 f \rightarrow 5d transitions. This approach employed wavefunction-based CASSCF/CASPT2 calculations at the spin–orbit level on Ce-centered embedded clusters. As shown in Fig. 6c, Ce³+ entering into Sc³+ site generates the largest energy level splitting giving the lowest energy transition of 23530 cm⁻¹ (425 nm). If this compound could be prepared, it would be ideal for application with violet or possibly blue LED chips. Calculating the electronic transition energy of Ce³+ entering the six-coordinated Na⁺ site also shows a red-shifted excitation spectrum of 25413 cm⁻¹ (393.5 nm). However, Ce³+ entering the largest Na⁺ polyhedral site shows the smallest energy level splitting with a transition energy estimated to be 26170 cm⁻¹ (382 nm). The blue shift compared to the other models stems from the large Na⁺ polyhedral volume giving rise to weaker crystal field splitting. These calculations are only \sim 12% underestimated compared to experimental results providing

additional support for the experimental assignment of Ce³⁺ entering into nominally dodecahedral Na⁺ site.

Conclusions

In summary, a combined theoretical and experimental investigation of β -K₂CO₃-type Na(Na_{0.5}Sc_{0.5})BO₃:Ce³⁺ was conducted to understand the relationship between structure and optical properties. The initial computational evaluation of this host suggested that Na(Na_{0.5}Sc_{0.5})BO₃ has a relatively high rigidity ($\Theta_D = 545 \text{ K}$) and sufficiently wide band gap $(E_{g,HSE} = 5.2 \text{ eV})$ to be a serviceable rare-earth substituted phosphor. The photoluminescent properties demonstrated that the resulting Na(Na_{0.5}Sc_{0.5})BO₃:Ce³⁺ phosphor has a blue emission peaking at 420 nm under ultraviolet 340 nm excitation. The observed luminescent properties and theoretical investigations indicated Ce³⁺ prefers to occupy the larger nominally eight-coordinated Na⁺ site rather than six-coordinated Na⁺ or Sc³⁺ sites. The local structure of the Ce³⁺-substituted site unexpectedly evolves into 9-coordination from 8-coordination, causing the optical properties to more closely match the NaMBO₃: Ce^{3+} (M = Sr, Ba) rather than NaMgBO₃:Ce³⁺. This work highlighted the importance of using experiment and computation to understand the relationship between crystal structure and luminescent properties when developing new inorganic phosphors.

Acknowledgments

The authors thank the National Natural Science Foundation of China (Nos. 51702057 and 11604002) and the National Science

Table II. Lattice parameters of the PBE0 functional optimized crystal structure containing different types of defect in the substituted and the unsubstituted $Na(Na_0.sSc_0.s)BO_3$ unit cell.

Defect type	a (Å)	b (Å)	c (Å)	α (°)	β (°)	γ (°)	$V(\mathring{A}^3)$
Un-substituted	10.071	8.980	13.853	90.2	123.3	89.9	1047.138
Ce_{Sc}	10.105	9.044	14.001	89.8	123.1	90.1	1071.829
$Ce_{Na(dod)} \bullet \bullet + Na_{Sc}''$	10.156	9.009	14.070	88.9	123.7	90.2	1070.579
$Ce_{Na(oct)} \bullet \bullet + Na_{Sc}''$	10.198	8.930	14.638	88.2	124.9	90.3	1092.162

Foundation (DMR 1847701). This research used the Maxwell/ Opuntia/Sabine cluster(s) operated by the University of Houston and the Research Computing Data Core (RCDC).

ORCID

Jakoah Brgoch https://orcid.org/0000-0002-1406-1352

References

- 1. E. F. Schubert, Science, 308, 1274 (2005).
- 2. S. Pimputkar, J. S. Speck, S. P. DenBaars, and S. Nakamura, Nat. Photonics, 3, 180 (2009).
- 3. P. Pust, P. J. Schmidt, and W. Schnick, Nat. Mater., 14, 454 (2015).
- 4. X. Huang, Nat. Photonics, 8, 748 (2014).
- 5. G. J. Hoerder et al., Nat. Commun., 10, 1824 (2019).
- H. Tottel et al., *Nat. Commun.*, 18, 1924 (2012).
 H. Zhu et al., *Nat. Commun.*, 5, 4312 (2014).
 P. Pust, V. Weiler, C. Hecht, A. Tücks, A. S. Wochnik, A. K. Henß, D. Wiechert, C. Scheu, P. J. Schmidt, and W. Schnick, Nat. Mater., 13, 891 (2014).
- 8. Z. Xia and Q. Liu, Prog. Mater Sci., 84, 59 (2016).
- 9. X. Qin, X. Liu, W. Huang, M. Bettinelli, and X. Liu, Chem. Rev., 117, 4488 (2017).
- 10. C. C. Lin and R. Liu, J. Phys. Chem. Lett., 2, 1268 (2011).
- 11. G. Li, Y. Tian, Y. Zhao, and J. Lin, Chem. Soc. Rev., 44, 8688 (2015).
- 12. Z. Xia and A. Meijerink, Chem. Soc. Rev., 46, 275 (2017).
- 13. L. Wang, R. Xie, T. Suehiro, T. Takeda, and N. Hirosaki, Chem. Rev., 118, 1951
- 14. X. Zhou, J. Qiao, and Z. Xia, Chem. Mater., 33, 1083 (2021).
- 15. L. Lin, L. Ning, R. Zhou, C. Jiang, M. Peng, Y. Huang, J. Chen, Y. Huang, Y. Tao, and H. Liang, *Inorg. Chem.*, 57, 7090 (2018).
- 16. J. E. Lee, B. B. Kim, Y. C. Park, and C. W. Won, Korean J. Mater. Res., 14, 885 (2004)
- 17. S. Li et al., Chem. Mater., 30, 494 (2018).

- 18. L. Wu, Y. Zhang, Y. F. Kong, T. Q. Sun, J. J. Xu, and X. L. Chen, *Inorg. Chem.*, 46, 5207 (2007).
- 19. X. Zhang, J. Song, C. Zhou, L. Zhou, and M. Gong, J. Lumin., 149, 69 (2014).
- 20. H. Yi, L. Wu, L. Wu, L. Zhao, Z. Xia, Y. Zhang, Y. Kong, and J. Xu, Inorg. Chem., 55, 6487 (2016).
- 21. W. R. Liu, C. H. Huang, C. P. Wu, Y. C. Chiu, Y. T. Yeh, and T. M. Chen, J. Mater. Chem., 21, 6869 (2011).
- 22. J. Zhong, W. Zhao, Y. Zhuo, C. Yan, J. Wen, and J. Brgoch, J. Mater. Chem. C, 7, 654 (2019).
- 23. J. Zhong, Y. Zhuo, S. Hariyani, W. Zhao, J. Wen, and J. Brgoch, Chem. Mater., 32, 882 (2020).
- 24. J. Hafner, J. Comput. Chem., 29, 2044 (2008).
- 25. G. Kresse and J. Furthmüller, *Phys. Rev. B*, **54**, 11169 (1996).
- 26. W. Kohn and L. J. Sham, Phys. Rev., 140, A1133 (1965).
- 27. G. Kresse and J. Hafner, Phys. Rev. B, 47, 558 (1993).
- 28. P. Hohenberg and W. Kohn, Phys. Rev., 136, B864 (1964).
- 29. J. Heyd, G. E. Scuseria, and M. Ernzerhof, J. Chem. Phys., 118, 8207 (2003).
- 30. G. Karlström et al., *Comput. Mater. Sci.*, **28**, 222 (2003).
- 31. Z. Barandiarán and L. Seijo, J. Chem. Phys., 89, 5739 (1988).
- 32. P. E. M. Siegbahn, J. Almlöf, A. Heiberg, and B. O. Roos, J. Chem. Phys., 74, 2384 (1981)
- 33. J. Fang, X. Zhang, J. Yao, G. Zhang, and K. Wang, Acta Crystallogr. Sect. E Struct. Reports Online, **68**, i36 (2012).
 34. J. Brgoch, S. P. DenBaars, and R. Seshadri, *J. Phys. Chem. C*, **117**, 17955 (2013).
- 35. A. C. Duke, S. Hariyani, and J. Brgoch, Chem. Mater., 30, 2668 (2018).
- Y. Zhuo, A. Mansouri Tehrani, A. O. Oliynyk, A. C. Duke, and J. Brgoch, Nat. Commun., 9, 4377 (2018).
- 37. S. Hariyani, A. C. Duke, T. Krauskopf, W. G. Zeier, and J. Brgoch, Appl. Phys. Lett., 116, 051901 (2020).
- 38. Y. Zhuo, A. Mansouri Tehrani, and J. Brgoch, J. Phys. Chem. Lett., 9, 1668 (2018).
- 39. J. Zhong, W. Zhao, F. Du, J. Wen, W. Zhuang, R. Liu, C. K. Duan, L. Wang, and K. Lin, J. Phys. Chem. C, 122, 7849 (2018).
- 40. Z. Xia and R. Liu, J. Phys. Chem. C, 116, 15604 (2012).